

Relation of local Cu^{2+} spins, crystal microstructure, and charge transport in the CuO_2 plane in $\text{Bi}_2\text{Sr}_2\text{CuO}_y$

Mao Zhiqiang, Tian Mingliang, Xu Yunhua, Yu Weijie, and Xu Cunyi

Structure Research Laboratory, University of Science and Technology of China, Hefei, Anhui 230026, People's Republic of China

Wang Ruiping and Wang Yu

Department of Physics, University of Science and Technology of China, Hefei, Anhui 230026, People's Republic of China

Zhang Yuheng

Chinese Center of Advanced Science and Technology (World Laboratory), P.O. Box 8730, People's Republic of China and Structure Research Laboratory, University of Science and Technology of China, Hefei, Anhui 230026, People's Republic of China

(Received 4 August 1994; revised manuscript received 22 December 1994)

Single-phase $\text{Bi}_2\text{Sr}_2\text{CuO}_y$ samples with a Sr deficiency were synthesized. Resistivity measurements have shown that a decrease in Sr concentration causes the 2201 phase to change from a metal to an insulator. Changes in the structural modulation of the 2201 phase, which accompany the metal-to-insulator transition, were examined. The experimental data indicate that the modulation periodicity reduces with a decrease in Sr concentration. The Raman-scattering analysis showed that the structural distortion of the 2201 phase is enhanced with a decrease in the modulation periodicity. In addition, the behavior of localized Cu^{2+} spins at the metal-insulator transition and its relation to the structural distortion were studied by means of electron paramagnetic resonance. The experimental data reveal that the fraction of localized Cu^{2+} spins increased appreciably with the occurrence of the metal-insulator transition. The relationship between the localized Cu^{2+} spins associated with the structural distortion and charge transport in the CuO_2 layer is discussed, based on these experimental results.

I. INTRODUCTION

Investigations of the properties of many oxide high- T_c superconductors have revealed a common characteristic, i.e., they have a CuO_2 plane in their structure. Within the range of lower carrier density where samples exhibit insulating behavior,¹ the localized Cu^{2+} spins are correlated antiferromagnetically in the CuO_2 plane. Shirane and co-workers² found that the long-range correlation of Cu^{2+} spins, i.e., spin fluctuation, exists even in the normal state of superconducting samples. Many authors believe that the origin of high- T_c superconductivity is related to this type of spin fluctuation.³⁻⁵ Nevertheless, at present there have been few experiments to reveal the relation which exists between spin fluctuation and charge transport in the CuO_2 plane.

On the other hand, it is known that high- T_c superconductors exhibit a strong sensitivity to the local structure due to a short coherent length. As a result, it can be expected that the spin fluctuation should also depend on the crystal microstructure.

An electron paramagnetic resonance (EPR) measurement is effective for determining the localized Cu^{2+} spin character. Information is obtained on the g value from the resonance field, on the spin relaxation time from the signal width, and on the susceptibility from the integrated intensity of the absorption signal. Thus the EPR method should be useful for studying the dependence of the localization of Cu^{2+} spins on microstructural characteristics. In previous work,⁶ we indicated that trans-

port properties in the CuO_2 plane are controlled by the crystalline microstructure. For example, in $\text{Bi}_2\text{Sr}_{2-x}\text{Ba}_x\text{CuO}_y$,^{6,7} we found that the structural distortion induced by the substitution of Ba for Sr resulted in the metal-insulator transition. Also we deduced that the real origin of the metal-insulator transition was the enhancement in the degree of localization of Cu 3d electrons caused by the structural distortion. Unfortunately, changes in the localized Cu^{2+} spins could not be observed directly by means of an EPR spectrum, since no EPR signal was detected above 90 K in the Ba-doped system. However, for the single-phase $\text{Bi}_2\text{Sr}_2\text{CuO}_y$ samples with Sr deficiency recently synthesized, in which the change in structure and physical properties were extremely similar to those in the Ba-doped system, a strong EPR signal for the Cu^{2+} was observed. Hence an investigation of the relation of Cu^{2+} spins, structural distortion, and charge transport in the CuO_2 plane can be conducted in this system.

II. EXPERIMENTAL METHODS

Samples were prepared by the conventional solid-state reaction method. Powders of Bi_2O_3 , SrCO_3 , MgO , and CuO were mixed with nominal compositions of $\text{Bi}_2\text{Sr}_{2-x}\text{Mg}_x\text{CuO}_y$ ($x=0.1, 0.2, 0.3, 0.4, 0.5, 0.6,$ and 0.7) and then preheated in air at 830°C . In order to ensure the complete reaction of the reactant oxides, the products were reground and reheated at 830°C . Preheating took place for 50 h. Then the powders were pressed

into pellets, sintered in air at 850°C for 50 h, and finally quenched in air. It should be mentioned here that our goal is to prepare the Mg-substituted 2201 phase, but the experimental results given below show that Mg atoms do not enter the 2201 structure and that they are separate from the mixture in preheating. The prepared samples can actually be described by $\text{Bi}_2\text{Sr}_{2-x}\text{CuO}_y$.

Powder x-ray diffraction (XRD) and electron diffraction (ED) were used to characterize the structure of these samples. The relative composition of these samples was analyzed using the x-ray photoelectron spectra (XPS) measured on an ESCALAB MKII surface analysis system. Raman spectra, measured on a Spex-1403 Raman spectrophotometer at room temperature, were used to determine the structural distortion associated with the change in the incommensurate modulation. The EPR experiments were carried out at 97 K by a Bruker (ER-200D-SRC) reflection x-band-type spectrometer. The frequency and magnetic field were measured by a frequency counter and a proton NMR gaussmeter, respectively. The resistivity of these samples was measured using a standard four-probe method.

III. EXPERIMENTAL RESULTS

A. XRD and composition analyses for the $\text{Bi}_2\text{Sr}_{2-x}\text{CuO}_y$ samples

Figure 1 shows the change of the XRD patterns with composition for the $\text{Bi}_2\text{Sr}_{2-x}\text{CuO}_y$ samples. From Fig. 1, curve *a*, it can be noted that for the sample with $x=0.1$ the (001) diffraction peaks split into doublets though $\text{Bi}_2\text{Sr}_2\text{CuO}_y$ (called the 2201 phase below) with $c=24 \text{ \AA}$ is the major phase. A previous study⁷ indicated that the splitting behavior for the (001) reflection origi-

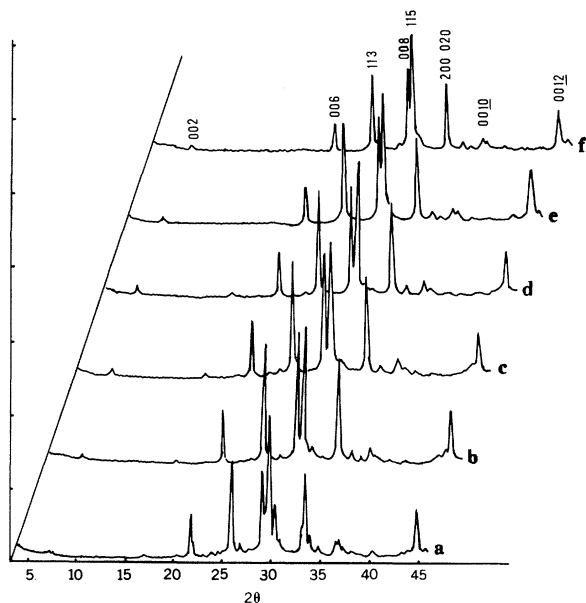


FIG. 1. XRD patterns of the $\text{Bi}_2\text{Sr}_{2-x}\text{CuO}_y$ samples; curve *a*, $x=0.1$; curve *b*, $x=0.2$; curve *c*, $x=0.3$; curve *d*, $x=0.4$; curve *e*, $x=0.6$; curve *f*, $x=0.7$.

nates from the presence of an insulating 2201 phase, with $c=12 \text{ \AA}$. For the samples with $x > 0.1$, the XRD patterns show that the occurrence of the insulating 2201 phase with $c=12 \text{ \AA}$ is suppressed and the samples exhibit the 2201 single phase. Table I gives the lattice constants for samples with $x=0.1, 0.3, 0.4, 0.6$, and 0.7 obtained from a least-squares refinement. It can be seen that the a and b axis lengths increase rapidly with a decrease in Sr concentration, while the length of the c axis decreases.

Table II gives the relative compositions of the samples with $x=0.1, 0.2, 0.3, 0.4$, and 0.5 measured by XPS. It shows that the compositions of these samples are all Sr deficient compared with the stoichiometric $\text{Bi}_2\text{Sr}_2\text{CuO}_y$. The XPS analysis also revealed that elemental Mg was not detected at either the surface or interior of these samples. It implies that the Mg atoms do not enter the lattice of the 2201 phase. In fact, the separation of elemental Mg at the bottom of the crucible was observed in the process of preheating. The actual composition of the as-prepared sample can be expressed as $\text{Bi}_2\text{Sr}_{2-x}\text{CuO}_y$ based on the data shown in Table II. Chakoumakos and co-workers have used the nominal composition of $\text{Bi}_2\text{Sr}_{2-x}\text{CuO}_y$ ($x=0.1-0.5$) to synthesize the 2201 sample.^{8,9} They found that the ideal 2201 single phase can be obtained and that the actual composition of the sample was also identified as $\text{Bi}_2\text{Sr}_{2-x}\text{CuO}_y$. This suggests that the "ideal" 2201 phase is deficient in Sr with a range of Sr deficiency ($\text{Bi}_2\text{Sr}_{2-x}\text{CuO}_y$, $x=0.1-0.5$). So for the $\text{Bi}_2\text{Sr}_{2-x}\text{CuO}_y$, it can be considered that there exist vacancies in the Sr sites and that the number of Sr vacancies should increase with a decrease in Sr concentration. However, although vacancies exist in Sr sites of $\text{Bi}_2\text{Sr}_{2-x}\text{CuO}_y$, we cannot rule out the possibility that a tiny fraction of Bi atoms occupies Sr sites. But it can be believed that the ratio of Bi occupation in Sr sites is far smaller than that of Sr vacancies in $\text{Bi}_2\text{Sr}_{2-x}\text{CuO}_y$. If the ratio of Bi occupation in Sr sites is larger than that of Sr vacancies, the elemental Cu in the composition shown in Table II is excessive and the excess Cu should be in a second phase of the sample. No second phase was detected in the $\text{Bi}_2\text{Sr}_{2-x}\text{CuO}_y$ sample within the limits of experiment accuracy, as shown in the XRD pattern in Fig. 1. Thus the change in the lattice constants of the 2201 phase shown in Table I can only be attributed to an increase in Sr vacancies.

B. ED analyses of the $\text{Bi}_2\text{Sr}_{2-x}\text{CuO}_y$ samples

Figures 2(a)–2(d) show the [100]-zone-axis ED patterns of the $\text{Bi}_2\text{Sr}_{2-x}\text{CuO}_y$ samples with $x=0.1, 0.3, 0.5$, and 0.7 . The satellite sequences reflect the conventional

TABLE I. Structure parameters of the $\text{Bi}_2\text{Sr}_{2-x}\text{CuO}_y$ samples (the error for the lattice constants is about 2/1000).

x	0.1	0.3	0.4	0.5	0.7
a (Å)	5.372	5.382	5.386	5.401	5.414
b (Å)	5.367	5.379	5.384	5.430	5.435
c (Å)	24.573	24.528	24.536	24.349	24.338

TABLE II. Relative composition of the $\text{Bi}_2\text{Sr}_{2-x}\text{CuO}_y$ samples.

x	0.1	0.20	0.3	0.4	0.5
Sr/Bi	0.9436	0.8961	0.8420	0.7992	0.7684
Cu/Bi	0.4813	0.4529	0.4642	0.4315	0.4643

monoclinic incommensurate-modulation structure of the 2201 phase. From the four ED patterns, the corresponding modulation vectors in the b^*-c^* plane, $q = \beta b^* + \gamma c^*$, can be identified

$$q_1^* = 0.20b^* - 0.32c^* \quad (x = 0.1),$$

$$q_2^* = 0.21b^* + 0.40c^* \quad (x = 0.3),$$

$$q_3^* = 0.22b^* - 0.70c^* \quad (x = 0.5),$$

$$q_4^* = 0.23b^* + 0.95c^* \quad (x = 0.7).$$

[The estimated error for the modulation vector is $\Delta\beta$ ($\Delta\gamma$) < 0.005 .] It is apparent that both the b^* and c^* components of the modulation vector increase remarkably with a decrease in Sr content, and the variation of the c^* component is larger than that of the b^* component. This suggests that the wavelength of the incommensurate modulation along the b and c axes reduces with decreasing Sr content.

C. Raman-scattering analyses for the $\text{Bi}_2\text{Sr}_{2-x}\text{CuO}_y$ samples

Figure 3 shows the Raman spectra of the $\text{Bi}_2\text{Sr}_{2-x}\text{CuO}_y$ samples with $x = 0.1, 0.2, 0.3, 0.4, 0.6,$ and 0.7 . For the samples with $x = 0.1, 0.2, 0.3,$ and 0.4 , two strong Raman modes at 456 and 622 cm^{-1} can be clearly observed, whose lines broaden slightly with a decrease in Sr content. However, for the samples with

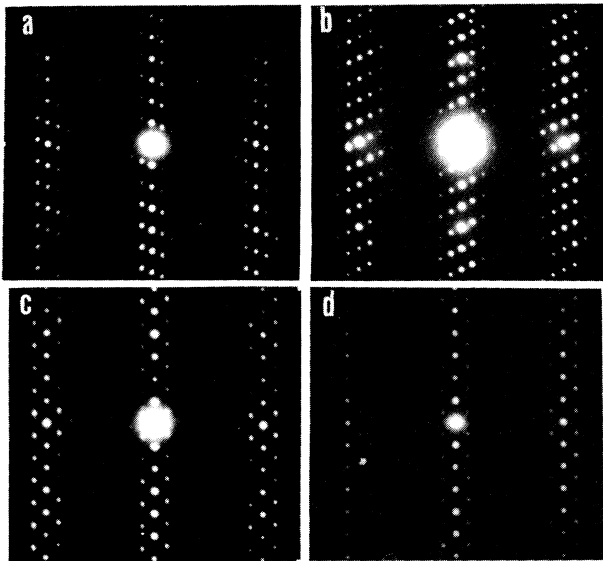


FIG. 2. (a) and (c), $[\bar{1}00]$ -zone-axis ED patterns of the $\text{Bi}_2\text{Sr}_{2-x}\text{CuO}_y$ samples with $x = 0.1$ and 0.5 ; (b) and (d), $[100]$ -zone-axis ED patterns of the $\text{Bi}_2\text{Sr}_{2-x}\text{CuO}_y$ samples with $x = 0.3$ and 0.7 .

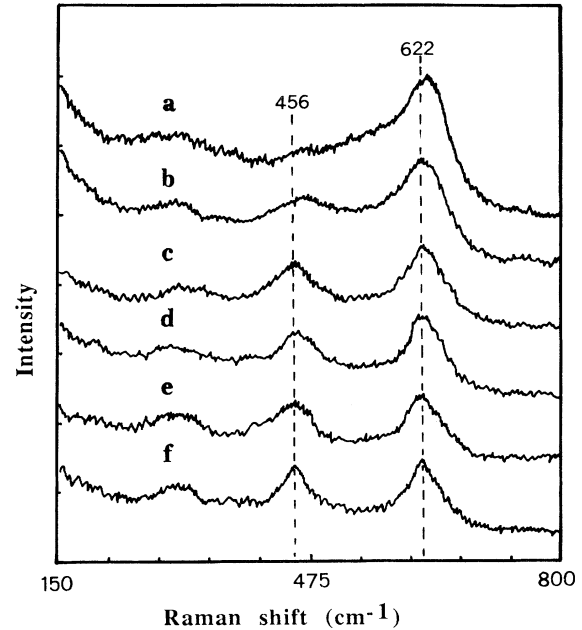


FIG. 3. Raman spectra of the $\text{Bi}_2\text{Sr}_{2-x}\text{CuO}_y$ samples; curve a, $x = 0.7$; curve b, $x = 0.6$; curve c, $x = 0.4$; curve d, $x = 0.3$; curve e, $x = 0.2$; curve f, $x = 0.1$.

$x = 0.6$ and 0.7 , the two lines broaden so significantly that they overlap each other in the frequency range of 456 – 622 cm^{-1} . The phonon modes observed in the Raman spectra of the $\text{Bi}_2\text{Sr}_{2-x}\text{CuO}_y$ samples can be assigned in accordance with the assignment of phonon Raman modes of the 2201 phase in Refs. 10 and 11. That is, the 622 and 456 cm^{-1} lines correspond, respectively, to the A_g vibrational mode of O_{Bi} atoms along the a axis and to the A_g vibrational mode of O_{Sr} atoms along the c axis (O_{Bi} and O_{Sr} refer to the oxygen atoms in the Bi_2O_2 and SrO layers).

There is little doubt that the broadening shown in Fig. 3 is related to a structural distortion associated with a change in the incommensurate modulation. In accordance with the results in Refs. 6 and 7, it can be stated that in the $\text{Bi}_2\text{Sr}_{2-x}\text{CuO}_y$ system the structure distortion is enhanced with a decrease in modulation wavelength. In this case, the Cu-O bond distance should change significantly. We have already determined that in the $\text{Bi}_2\text{Sr}_{2-x}\text{CuO}_y$ system the a and b axis lengths increase with decreasing Sr content. In general, the a and b axis lengths are considered to be controlled by the in-plane Cu-O bond distance.¹² Thus the increase of a and b axis lengths actually reflects a distortion of the Cu-O bond. Unfortunately, such a change in the Cu-O bond distance with the modulation structure cannot be detected directly by Raman scattering, since the copper and oxygen atoms in the CuO_2 layers are not Raman active in the 2201 phase.

D. Resistivity of the $\text{Bi}_2\text{Sr}_{2-x}\text{CuO}_y$ samples

The temperature dependence of $\ln\rho$ (ρ is the resistivity) of the $\text{Bi}_2\text{Sr}_{2-x}\text{CuO}_y$ samples ($x = 0.1, 0.2, 0.3, 0.4, 0.5,$

0.6, and 0.7) is shown in Fig. 4. Although all the samples, except for $x=0.1$, exhibit the ideal 2201 single phase, the charge-transport properties reflected in Fig. 4 are noticeably different. The $x=0.1$ sample exhibits metallic behavior within the temperature range of 7–300 K and no superconductivity is observed, while other samples with $x > 0.1$ exhibit semiconductivity. Furthermore, the resistivity of the samples increases rapidly with decreasing Sr content. For the sample with $x=0.7$, the resistivity is 7–8 orders of magnitude larger than that of the sample with $x=0.1$. It can be seen that the 2201 phase changes from metal to insulator with a decrease in Sr content.

E. EPR signal for the $\text{Bi}_2\text{Sr}_{2-x}\text{CuO}_y$ samples

Figure 5 shows the EPR signal at 97 K of the $\text{Bi}_2\text{Sr}_{2-x}\text{CuO}_y$ samples with $x=0.1, 0.2, 0.3, 0.4, 0.5, 0.6,$ and 0.7 . The g factor corresponding to these lines is approximately 2.1, indicating the dominance of Cu^{2+} spins. In previous EPR investigations of high- T_c superconductors, some authors attributed the EPR signal observed in the 0.3–0.35 T range to localized Cu^{2+} ions which do not participate in superconductivity (at grain boundaries, for instance) or to a small amount of Cu^{2+} -based impurities.^{13,14} But Ishida and co-workers found that the EPR signal coming from Cu^{2+} spins reproduced the intrinsic susceptibility of the high- T_c superconducting phase.¹⁵ This implied that the EPR signal in the 0.3–0.35 T range comes from localized Cu^{2+} spins in the superconducting phase, not from an impurity phase. From the EPR lines shown in Fig. 4, we believe that the argument of Ishida *et al.* is reasonable. The results shown in Fig. 1 reveal that no impurity appears in the samples with $x > 0.1$. Nevertheless, the relative intensity of the EPR line shown in Fig. 5 increases rapidly with a decrease in Sr content. Obviously, we cannot ascribe this

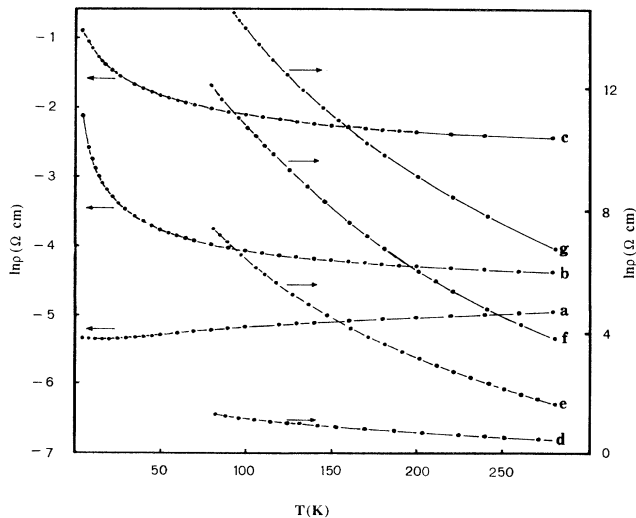


FIG. 4. Temperature dependence of $\ln \rho$ (ρ is the resistivity) of the $\text{Bi}_2\text{Sr}_{2-x}\text{CuO}_y$ samples; curve a , $x=0.1$; curve b , $x=0.2$; curve c , $x=0.3$; curve d , $x=0.4$; curve e , $x=0.5$; curve f , $x=0.6$; curve g , $x=0.7$.

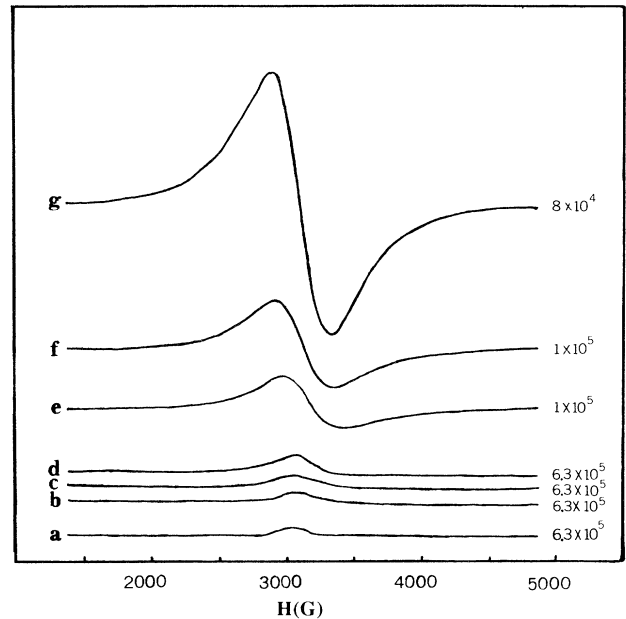


FIG. 5. EPR spectra at 97 K of the $\text{Bi}_2\text{Sr}_{2-x}\text{CuO}_y$ samples; curve a , $x=0.1$; curve b , $x=0.2$; curve c , $x=0.3$; curve d , $x=0.4$; curve e , $x=0.5$; curve f , $x=0.6$; curve g , $x=0.7$.

behavior to an increase of an impurity phase. In accordance with the argument of Ishida *et al.*, we conclude that the fraction of localized Cu^{2+} spins increases strikingly with a decrease in Sr content in the 2201 phase.

IV. DISCUSSION

From the experimental results described above, it is apparent that the change in structure and charge-transport properties caused by a decrease in Sr composition in $\text{Bi}_2\text{Sr}_{2-x}\text{CuO}_y$ is extremely similar to the behavior observed in the $\text{Bi}_2\text{Sr}_{2-x}\text{Ba}_x\text{CuO}_y$ system.⁶ For the $\text{Bi}_2\text{Sr}_{2-x}\text{Ba}_x\text{CuO}_y$ system, we proposed that an intensification of the structural distortion causes the Cu 3d electrons to change from a partially delocalized to a localized state, which accounts for the metal-insulator transition in this system. The experimental results from the $\text{Bi}_2\text{Sr}_{2-x}\text{CuO}_y$ system are in accordance with this argument. In $\text{Bi}_2\text{Sr}_{2-x}\text{CuO}_y$, it is apparent that the fraction of localized Cu^{2+} spins increases markedly with the change from metal to insulator. Therefore it can be assumed that the metal-insulator transition in $\text{Bi}_2\text{Sr}_{2-x}\text{CuO}_y$ also results from a change in the degree of localization of the Cu 3d electrons induced by the structural distortion.

In the literature, many authors have stressed the importance of an antiferromagnetic (AF) spin fluctuation in the high- T_c cuprates.^{3–5} Many anomalies in the normal-state properties of high- T_c superconductors can be explained in terms of AF spin fluctuations of two-dimensional itinerant-electron systems. The above-mentioned experimental results are best understood using the spin-fluctuation theory. In the samples with $x=0.4, 0.5, 0.6,$ and 0.7 , which exhibit nearly insulating

behavior, one can imagine that an AF spin correlation among Cu^{2+} ions exists, since a large number of the Cu 3d electrons are in a localized state. Secondly, in samples with $x=0.3$ and 0.2 which exhibit semiconductivity, the AF spin correlation is weaker due to a decrease in the number of localized Cu^{2+} spins. Thus, in the $x=0.1$ sample exhibiting metallic behavior, it may be deduced that the AF spin fluctuations occur though the AF order with large range disappears. This deduction seems to support the argument that charge transport in the CuO_2 planes is determined by spin scattering.¹⁶

In accordance with the above discussion, we think that the occurrence of high- T_c superconductivity is closely related to the following factors. (1) In the normal state of high- T_c superconductors, the Cu 3d electrons are in partially localized states. A fraction of the Cu 3d electrons are likely to participate in charge transport. Furthermore, the degree of the localization of the Cu 3d electrons should be dependent upon temperature. This idea may explain anomalies in the normal-state properties of high- T_c superconductors. (2) In the normal state, weak spin fluctuations may exist, as well as electric and magnetic correlations between spin fluctuations and itinerant carriers.

It is obvious that, in the $\text{Bi}_2\text{Sr}_{2-x}\text{CuO}_y$ system, the change in state of Cu 3d electrons can be attributed to the microstructural distortion induced by a decrease in Sr content. ED and Raman-scattering analysis have revealed that the structural distortion in the Sr-deficient 2201 phase intensifies with a decrease in the modulation wavelength, thus resulting in a distortion of the Cu-O bond. The distortion in the Cu-O bond changes the hybridizing of the Cu 3d-O 2p state, thus enhancing the degree of localization of Cu 3d electrons. Consequently,

we can say that in the $\text{Bi}_2\text{Sr}_{2-x}\text{CuO}_y$ system the fraction of localized Cu^{2+} spins increases with a decrease in the modulation wavelength. In other words, the state of Cu 3d electrons is controlled by the microstructural characteristics. This view agrees well with the argument proposed in Ref. 6.

V. CONCLUSION

We have studied the microstructure, transport properties, and change in the state of Cu 3d electrons of the $\text{Bi}_2\text{Sr}_{2-x}\text{CuO}_y$ system by means of XRD, ED, resistivity measurement, and EPR spectrum. Furthermore, the relationship between the state of Cu 3d electrons and the structural distortion and charge transport in the CuO_2 plane was discussed. From these experimental investigations and analyses, the following conclusion may be drawn.

(1) The normal-state resistivity of high- T_c cuprates is dependent upon the degree of localization of the Cu 3d electrons (i.e., the number of localized Cu^{2+} spins). This implies that charge transport in the CuO_2 plane is determined by spin scattering.

(2) The state of Cu 3d electrons is related to the crystal microstructure. The Cu 3d electrons change from a partially delocalized to a localized state with an increase of the structural distortion.

ACKNOWLEDGMENTS

This research was supported by the National Center for Research and Development on Superconductivity and the Doctoral Fund of National Education Committee of China.

¹*Physical properties of High-Temperature superconductors I*, edited by D. M. Ginsberg (World Scientific, Singapore, 1989).

²G. Shirane, Y. Endoh, R. Birgeneau, M. A. Kastner, Y. Hidaka, M. Oda, M. Suzuki, and T. Murakami, *Phys. Rev. Lett.* **59**, 1613 (1987).

³T. Moriya, Y. Fakahashi, and K. Ueda, *J. Phys. Soc. Jpn.* **59**, 2905 (1990).

⁴A. J. Millis, H. Monien, and D. Pines, *Phys. Rev. B* **42**, 167 (1990).

⁵P. Monthoux and D. Pines, *Phys. Rev. B* **49**, 4261 (1994).

⁶Z. Q. Mao, M. L. Tian, M. R. Ji, J. S. Zhu, J. Zuo, R. P. Wang, Y. Wang, and Y. H. Zhang, *Phys. Rev. B* **49**, 9857 (1994).

⁷Z. Q. Mao, C. G. Fan, L. Shi, Z. Yao, L. Yang, Y. Wang, and Y. H. Zhang, *Phys. Rev. B* **47**, 14 467 (1993).

⁸B. C. Chakoumakos, P. S. Eby, B. C. Sales, and Edward Sonder, *J. Mater. Res.* **4**, 767 (1989).

⁹Edward Sonder, B. C. Chakoumakos, and B. C. Sales, *Phys.*

Rev. B **40**, 6872 (1989).

¹⁰M. Cardona, C. Thomsen, R. Liu, H. G. Vonscherner, M. Hartwey, Y. F. Yan, and Z. X. Zhao, *Solid State Commun.* **66**, 1225 (1988).

¹¹R. Liu, M. Klein, P. D. Han, and D. A. Payne, *Phys. Rev. B* **45**, 7392 (1992).

¹²P. Mandal, A. Poddar, and B. Ghosh, *Phys. Rev. B* **43**, 13 102 (1991).

¹³K. Tagaya, N. Fukuoka, and Nakanishi, *Jpn. J. Appl. Phys.* **29**, 868 (1990).

¹⁴Y. Hayashi, M. Fukui, H. Sasakura, S. Minamigawa, T. Fujita, and K. Nakahigashi, *Jpn. J. Appl. Phys.* **28**, 759 (1989).

¹⁵T. Ishida, K. Koga, S. Nakamura, Y. Lye, K. Kanoda, S. Okui, T. Takahashi, T. Oashi, and K. Kumagai, *Physica C* **176**, 24 (1991).

¹⁶T. Ito, K. Takenaka, and S. Uchida, *Phys. Rev. Lett.* **70**, 3995 (1993).

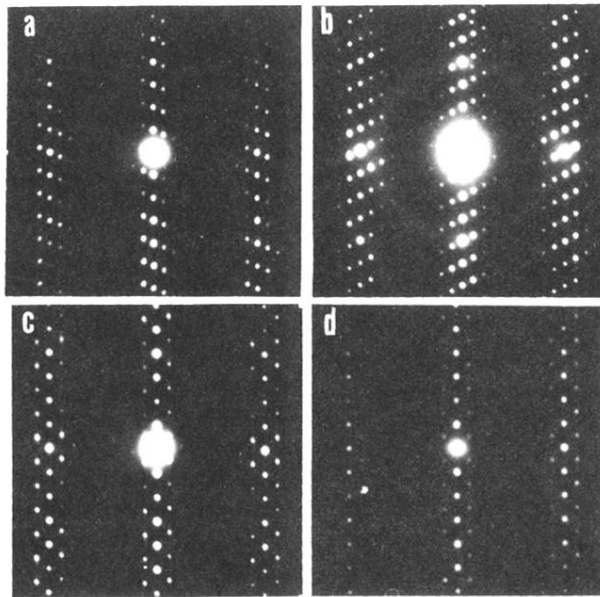


FIG. 2. (a) and (c), $[100]$ -zone-axis ED patterns of the $\text{Bi}_2\text{Sr}_{2-x}\text{CuO}_y$ samples with $x=0.1$ and 0.5 ; (b) and (d), $[100]$ -zone-axis ED patterns of the $\text{Bi}_2\text{Sr}_{2-x}\text{CuO}_y$ samples with $x=0.3$ and 0.7 .